Chinese Chemical Letters 35 (2024) 108930

Contents lists available at ScienceDirect

Chinese Chemical Letters

journal homepage: www.elsevier.com/locate/cclet

Keplerate polyoxomolybdate nanoball mediated controllable preparation of metal-doped molybdenum disulfide for electrocatalytic hydrogen evolution in acidic and alkaline media

Ping Wang[a], Ting Wang[a,*], Ming Xu[a], Ze Gao[b], Hongyu Li[a], Bowen Li[a], Yuqi Wang[a], Chaoqun Qu[a,*], Ming Feng[a,*]

[a] Key Laboratory of Functional Materials Physics and Chemistry of the Ministry of Education, Jilin Normal University, Changchun 130103, China
[b] School of Science, Changchun University of Science and Technology, Changchun 130022, China

ARTICLE INFO

Article history:
Received 19 June 2023
Revised 31 July 2023
Accepted 14 August 2023
Available online 18 August 2023

Keywords:
Polyoxometalate
Electrocatalytic
Hydrogen evolution reaction
Doping
MoS_2

ABSTRACT

Rationally designed novel cost-effective hydrogen evolution reaction (HER) electrocatalysts with controlled surface composition and advanced structural superiority is extremely critical to optimize the HER performance. Polyoxometalates (POMs) with structural diversity and adjustable element compositions represent a promising precursor for rational design and preparation of HER electrocatalysts. Herein, a series of transition metal-doped MoS_2 materials with different surface engineered structures (Fe, Cr, V doping and S vacancies) (M-MoS_2/CC, M = Fe, Cr and V) were fabricated by a simple hydrothermal-vulcanization strategy using Keplerate polyoxomolybdate nanoball ({$Mo_{72}Fe_{30}$}, {$Mo_{72}Cr_{30}$}, {$Mo_{72}V_{30}$}, {Mo_{132}}) as precursors. The enlarged interlayer spacing as well as the integration of homogeneous transition metal doping and abundant sulfur vacancies endows prepared M-MoS_2/CC with superior HER electrocatalytic performance and excellent long-term working stability in both acidic and alkaline media. The optimized Fe-MoS_2/CC afford current densities of 10 and 50 mA/cm^2 at overpotentials of 188/272 mV and 194/394 mV in 0.5 mol/L H_2SO_4 and 1.0 mol/L KOH aqueous solution, respectively, outperforming most of reported typical transition metal sulfide-based catalysts. This work represents an important breakthrough for POMs-mediated highly efficient transition metal sulfide-based HER electrocatalysts with wide range pH activity and may provide new options for the rational design of promising HER electrocatalysts and beyond.

© 2024 Published by Elsevier B.V. on behalf of Chinese Chemical Society and Institute of Materia Medica, Chinese Academy of Medical Sciences.

Hydrogen (H_2) is advocated as a promising clean fuel for next-generation power supply because of its high gravimetric specific energy density (120 MJ/kg) and carbon-free emission [1–5]. Electrocatalytic water splitting is a green hydrogen energy generation technology, which has sparked intensive research interest as an ideal sustainable system for the future [6,7]. Platinum (Pt) is regard as a benchmark catalyst for HER in acidic conditions, but it has still not been extensively utilized due to the low abundance and high cost. Furthermore, the HER reaction rate for Pt-based catalyst in alkaline media is 2–3 orders of magnitude lower than those in acidic solution [8,9]. Motivated by this challenge, great efforts have been devoted to explore the non-noble metal-based alternatives with low cost and high natural abundance [10–20].

Among many metal-based catalysts, transition metal sulfides (TMS) have been investigated greatly as a potential electrocatalyst for HER applications due to their low cost, attractive electronic properties and excellent stability [19]. MoS_2, as a typical 2D TMS possesses unique graphene like structure and proper $\triangle G_H{}^*$ value close to that of Pt. However, some central drawbacks including limited edge active sites, inferior intrinsic conductivity, complex preparation, as well as stability and solubility in acidic media restrict its widespread applications for HER [21–23].

Polyoxometalates (POMs), as a unique class of nanosized clusters have been used as ideal precursors for synthesis of MoS_2-based electrocatalyst owing to their exceptional structure and composition [24–27]. Although great efforts have been made, their performances are still not satisfying. The highly efficient POMs-derived catalysts for both acidic and alkaline environment still require to be reported and the advantages of POMs need to be further developed. In this regard, Keplerate polyoxomolybdate, as an important POMs family may be a good starting point due to

* Corresponding authors.
E-mail addresses: wangt@jlnu.edu.cn (T. Wang), quchaoqun@jlnu.edu.cn (C. Qu), mingfeng@jlnu.edu.cn (M. Feng).

https://doi.org/10.1016/j.cclet.2023.108930
1001-8417/© 2024 Published by Elsevier B.V. on behalf of Chinese Chemical Society and Institute of Materia Medica, Chinese Academy of Medical Sciences.

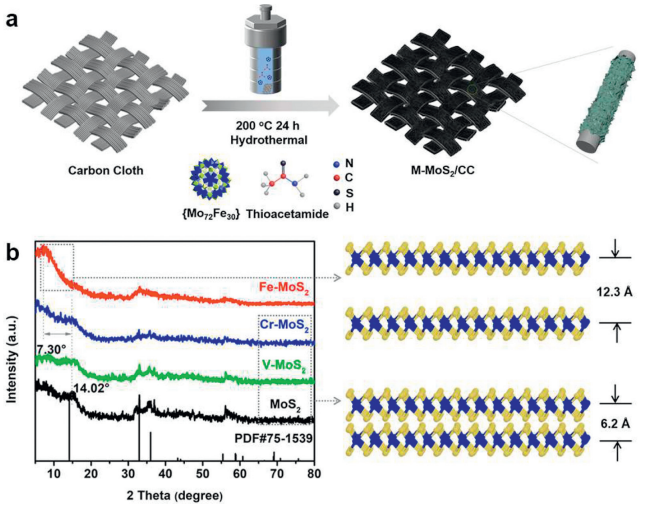

Fig. 1. (a) Illustration of the preparation of M-MoS_2/CC. (b) XRD patterns of M-MoS_2/CC. At the right, the structural models of MoS_2 with different interlayer spacings.

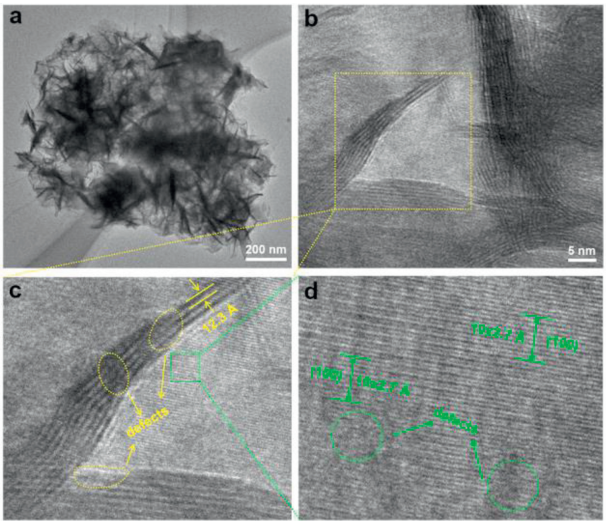

Fig. 2. (a) TEM and (b–d) high-resolution TEM (HRTEM) images of Fe-MoS_2/CC.

its unique electronic characteristics and spherical porous structure [28]. The porous spherical molybdenum oxide-based clusters possess a number of distinctive superiorities for designing MoS_2-based materials: (1) The well-defined molecular structures can provide homogeneous spatial distribution of Mo and other metals at the atomic scale; (2) The giant molecular spheres can achieve the incorporation of Mo and other metal sources at the single-molecule level; (3) The highly hydrophilic, solubility and gated pores in this discrete porous cluster can allow sufficient permeation and transportation of various sulfur source in aqueous solution, realizing the uniform vulcanization [29].

Motivated by above considerations, in this work, using a simple hydrothermal method, we developed a series of metal-doped molybdenum disulfide on carbon cloth (M-MoS_2/CC, M = Fe, Cr and V) as effective electrocatalysts for HER in both acidic and alkaline media, which were synthesized by one-step sulfuration of the Keplerate-type $\{Mo_{72}Fe_{30}\}$, $\{Mo_{72}Cr_{30}\}$, $\{Mo_{72}V_{30}\}$ clusters (Fig. 1a, Figs. S1 and S2 in Supporting information). MoS_2/CC was also prepared as comparison sample by using $\{Mo_{132}\}$ cluster as the precursor. As expected, the optimized M-MoS_2/CC catalysts display improved catalytic behavior due to homogeneous metal doping modification, the "highway" of charge transport, large surface area, and abundant active catalytic sites. In comparison to Cr-MoS_2/CC, V-MoS_2/CC and pure MoS_2/CC, the as-prepared Fe-MoS_2/CC presented lowest overpotentials of 188/272 mV and 194/394 mV to achieve the current density of 10 and 50 mA/cm^2 in acidic and alkaline media, respectively.

In Fig. 1b, the diffraction peaks located at 32.96°, 35.98° and 56.26° in the X-ray diffraction (XRD) patterns of M-MoS_2 are assigned to the (100), (102) and (106) crystal planes of hexagonal MoS_2 (PDF#75-1539). The slight deviation of individual diffraction peak may be ascribed to the transition metal doping. The peaks at 2θ = 14.02° in Cr-MoS_2, V-MoS_2 and MoS_2 match well with the (002) characteristic crystal plane, suggesting a stacked, multilayered structure with the interlayer spacing of 6.2 Å. However, this characteristic peak moves obviously to lower degree when the $\{Mo_{72}Fe_{30}\}$ was used as precursor. A new diffraction peak centered at 7.30° can be observed, which correspond to the 12.3 Å interlayer spacing based on the computational simulations. The differences in interlayer spacing for various M-MoS_2 samples may be attributed to the differences in doping content, type, and location. Compared with the standard pattern of MoS_2, some characteristic peaks are not presented, which may be attributed to the poor crystallinity of prepared catalysts. This is consistent with the reported literatures [26,27]. The Fe-MoS_2 materials synthetized at different temperatures also display the same phenomenon (Fig. S3 in Supporting information). The enlarged interlayer spacing could provide more accessible catalytic active sites during the electrochemical HER process.

The micromorphology of these as-prepared MoS_2-based catalysts was surveyed with scanning electron microscopy (SEM) technique (Figs. S4–S8 in Supporting information). It can be found that the treated carbon cloth displays smooth surface (Fig. S4) and well-arranged MoS_2 nanosheets grow uniformly on the surface of carbon cloth after one-step hydrothermal treatment. The elemental mapping images show that Mo, S, Fe, Cr and V elements are distributed homogeneously throughout corresponding M-MoS_2 samples while neither elemental segregation nor phase separation was observed, confirming the atomically precise metal doping. The corresponding element contents were confirmed by EDX analysis and summarized in Table S1 (Supporting information). Such unique nanostructure could increase the effective adsorption of hydrogen species and engender abundant defective sites for catalysis. Transmission electron microscopy (TEM) and high-resolution TEM (HRTEM) images in Fig. 2 offer more morphology information of Fe-MoS_2. As can be seen, the prepared Fe-MoS_2 exhibits thin nanosheets appearance with lots of wrinkles, which is in accordance with SEM result. The HRTEM images shown in Figs. 2b and c demonstrate a few layers stacked MoS_2 nanosheets with enlarged interlayer spacing of 12.3 Å and abundant edge defects. This structural feature can enlarge the specific surface area and expose more available inherent reaction active sites during the electrochemical reactions. As shown in Fig. 2d, the ordered crystal lattice with interplanar spacing of 0.27 nm was assignable to the (100) crystal planes of MoS_2 and while some lattice defects can be also observed, which is attributed to the introduction of foreign Fe elements [27].

Fig. 3a shows the Raman spectra of M-MoS_2/CC. Five obvious Raman peaks located at approximately 154, 200, 242, 289, and 342 cm^{-1} can be clearly identified in the spectra, which are assigned to the phonon modes in 1T-MoS_2, suggesting the information of metallic 1T-MoS_2 nanosheet instead of 2H-MoS_2 with poor charge transport properties. The zoomed-in spectra shown in Fig. S9 (Supporting information) exhibit peak width changes and slight peak shifts upon the foreign metal doping, illustrating that the introduction of secondary transition metals (Fe, Cr, and V) could tune the surrounding electronic properties of MoS_2 [26]. This re-

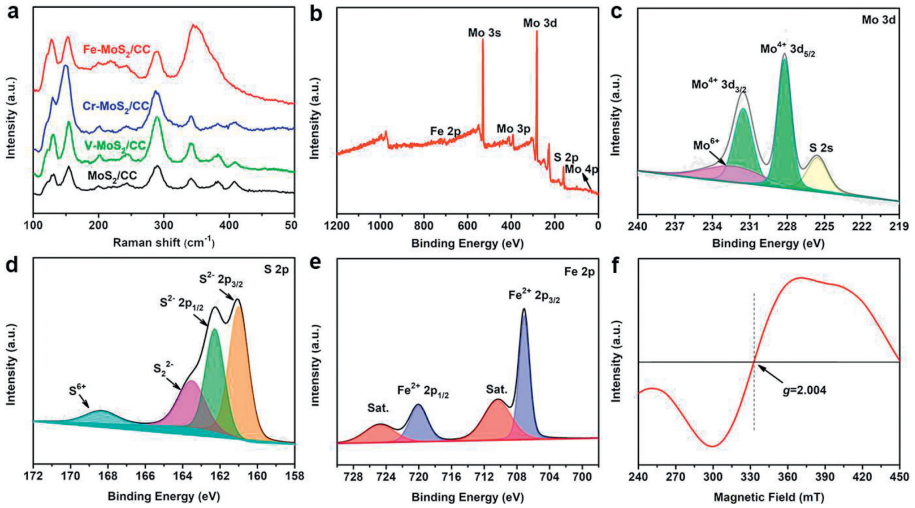

Fig. 3. (a) Raman spectra of M-MoS_2/CC. (b) The full XPS spectrum of Fe-MoS_2/CC. High-resolution XPS spectra of (c) Mo 3d, (d) S 2p and (e) Fe 2p in Fe-MoS_2/CC. (f) EPR spectrum of Fe-MoS_2.

sult can be also proved by their band gap structures. As shown in Fig. S10 (Supporting information), the band gaps (E_g) of Fe-MoS_2, Cr-MoS_2, V-MoS_2 and MoS_2 are estimated to be 1.641, 1.792, 1.852 and 1.875 eV, respectively. The band gaps of M-MoS_2 decreased compared to pure MoS_2, suggesting the regulated electronic structure and enhanced electron transfer characteristics after transition metal doping [30]. The conduction bands (CB) of these samples were further calculated from the first reduction applied potential in cyclic voltammetry (CV) curves shown in Fig. S11 (Supporting information). The CB energy level of MoS_2 was assigned to be −0.445 V *versus* Ag/AgCl electrode, corresponding to −0.248 V *versus* NHE, while the CB energy levels of Fe-MoS_2, Cr-MoS_2, V-MoS_2 were changed to −0.303 V, −0.29 V and −0.275 V *versus* NHE, respectively [31]. According to the above results, the corresponding energy level distribution of these as-prepared MoS_2-based catalysts was summarized in Fig. S12 (Supporting information). The energy-level difference ($\triangle E$) between the CB of MoS_2 and the reduction potential of $E(H^+/H_2)$ can reflect the electron injection dynamics [30,32]. The larger $\triangle E$ of M-MoS_2 than pure MoS_2 suggests that the foreign metal doping can endow MoS_2 with larger electron injection driving force to reduce the energy required for the activation of hydrogen and promote the electron transfer, which benefits to improve the electrocatalytic H_2 evolution. Moreover, Brunauer–Emmett–Teller (BET) specific surface area of Fe-MoS_2 was estimated to be 32.7 m^2/g (Fig. S13 in Supporting information), which is significantly higher than that of other catalysts, confirming that it can provide more highly accessible catalytic active sites for reactive intermediates.

The existence of different elements in corresponding samples is confirmed by the X-ray photoelectron spectroscopy (XPS) spectra (Figs. 3b–e and Figs. S14–S16 in Supporting information). As illustrated in Fig. 3c, the two prominent characteristic peaks centered at 228.2 eV and 231.6 eV are assigned to the Mo $3d_{5/2}$ and Mo $3d_{3/2}$ of Mo^{4+}, and the weak peak located at 232.6 eV belongs to the Mo^{6+}, which is attributed to the inevitable oxidation of Mo^{4+} on the catalyst surface after exposing to air [33]. The high-resolution S 2p spectrum exhibits four peaks at 161.0 eV and 162.3 eV, which are assigned to the S $2p_{3/2}$ and S $2p_{1/2}$ of S^{2-} for MoS_2, as well as 163.5 eV and 168.4 eV corresponding to S_2^{2-} and S^{6+}, respectively. The S^{6+} may be originated from the physically-absorbed sulfate from reaction precursor [26]. As illustrated in Fig. 3e, the Fe-MoS_2 exhibits oxidation states of Fe^{2+} with the binding energies of 707.1 and 720.1 eV, which are indexed into Fe $2p_{3/2}$ and Fe $2p_{1/2}$, respectively. The characteristic peaks at the binding energies of 710.5 and 724.7 eV correspond to the satellite peaks of Fe [34,35]. The electron paramagnetic resonance (EPR) spectra (Fig. 3f and Fig. S17 in Supporting information) show that all catalysts exhibit apparent characteristic signal at $g = 2.004$, which proves the presence of sulfur vacancies in M-MoS_2, which is in accordance with the TEM result [36]. Above characterizations prove the successful fabrication of Keplerate polyoxomolybdate mediated M-MoS_2 catalysts, the abundant structural defects and unique electron structure may endow M-MoS_2 with abundant catalytic active sites and suitable adsorption capacities for reaction intermediates in both acidic and alkaline media, thus facilitating the electrochemical reaction.

To investigate the HER electrocatalytic performance of as- prepared catalysts, the linear sweep voltammetry (LSV) measurements of M-MoS_2/CC with different metal doping in acidic media are firstly studied. As shown in Figs. 4a, Fe-MoS_2/CC delivers smaller overpotentials (188, 272, and 350 mV) compared with Cr-MoS_2/CC (212, 288, and 358 mV), V-MoS_2/CC (214, 292, and 366 mV) and MoS_2/CC (224, 308, and 388 mV) at 10, 50 and 100 mA/cm^2 in 0.5 mol/L H_2SO_4, respectively. The exceptional HER activity of these fabricated catalysts confirms the superiority of Keplerate polyoxomolybdate nanoball as precursors, especially for Fe-MoS_2/CC synthesized from $\{Mo_{72}Fe_{30}\}$ with enlarged interlayer spacing, which could expose and provide more catalytic active site during the HER process. In comparison, the LSV curves of bare CC and Fe-MoS_2/CC-T catalysts synthesized at different temperatures (160–200 °C) were also measured (Fig. S18a in Supporting information). The polarization curves show that the current densities increase with the elevation of reaction temperature. The Fe-MoS_2/CC-200 only demanded a lower overpotential compared to bare CC (270, 414, and 528 mV), Fe-MoS_2/CC-160 (228, 300, and 364 mV) and Fe-MoS_2/CC-180 (196, 276, and 350 mV) to drive the current density of 10, 50 and 100 mA/cm^2. Consequently, the best HER electrocatalytic performance is realized at a sulfidation temperature of 200 °C. These results are further repeated using graphite rod as counter electrode to exclude the effect of Pt. The graphite rod counter electrode yields very close HER performance to that of Pt counter electrode (Fig. S19 and Table S2 in Supporting information), ruling out the possibility of dissolving and deposition of Pt in the measurements. Tafel plots for Fe-MoS_2/CC-200 (166 mV/dec) shown in Fig. 4b is lower than that for Cr-MoS_2/CC-200 (177 mV/dec), V-MoS_2/CC-200 (189 mV/dec) and MoS_2/CC-200 (197 mV/dec), indicating the fast reaction kinetic process [37–39].

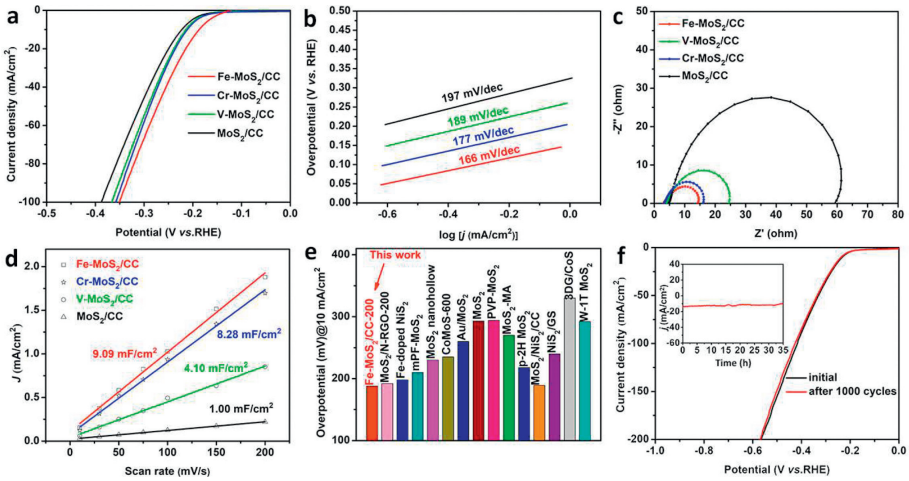

Fig. 4. (a) LSV curves, (b) Tafel plots, (c) EIS spectra and (d) C_{dl} values of M-MoS_2/CC in 0.5 mol/L H_2SO_4. (e) The comparison of overpotential at 10 mA/cm^2 to other typical metal sulfide catalysts in 0.5 mol/L H_2SO_4. (f) Polarization curves initially and after 1000 CV cycles (inset: the long-term durability tests for 35 h).

In the next step, electrochemical impedance spectroscopy (EIS) measurement was conducted to investigate the electrode kinetics and interfacial reaction of M-MoS_2/CC and MoS_2/CC for HER in 0.5 mol/L H_2SO_4. As shown in the EIS spectra (Fig. 4c), all catalysts show smooth semi-circle, and M-MoS_2/CC electrodes exhibit smaller series resistance and charge-transfer resistance (R_{ct}) than that of MoS_2/CC, which indicates that the enhanced HER electrocatalytic activity is attributed to transition metal doping. Sample Fe-MoS_2/CC has the lowest R_{ct} of *ca.* 11.6 Ω because of more exposed active sites, revealing the better electron transferability at the electrocatalyst/electrolyte interfaces and superior catalytic behavior [40–42]. In contrast, Fe-MoS_2/CC prepared at 160 and 180 °C present larger R_{ct} (Fig. S18c in Supporting information), suggesting the low conductivities and poorer HER catalytic activity. The electrochemical active surface area (ECSA) was further estimated from the electrochemical double-layer capacitance (C_{dl}), which was derived from the cyclic voltammetry (CV) curves at various scan rates (Fig. S20 in Supporting information) [43,44]. As shown in Fig. 4d, the C_{dl} values of Fe-MoS_2/CC, Cr-MoS_2/CC, V-MoS_2/CC and MoS_2/CC are calculated to be 9.09, 8.28, 4.10 and 1.00 mF/cm^2, respectively. The M-MoS_2/CC electrodes have larger C_{dl} value than that of MoS_2/CC, indicating that the foreign metal doping can effectively increase the ECSA during electrochemical process. Apparently, the Fe-MoS_2/CC delivers the highest C_{dl} value, which may result from the enlarged interlayer spacing, demonstrating that Fe-MoS_2/CC provides more accessible catalytic active sites on the surface. Therefore, Fe-MoS_2/CC electrode results in a better electrochemical HER performance among all the prepared catalysts. Besides, the HER electrocatalytic performance of Fe-MoS_2/CC electrode is also superior to most recently reported transition metal sulfide catalysts (Fig. 4e and Table S3 in Supporting information). To ultimately evaluate the long-term stability of prepared catalysts, the multiple CV cycles and chronoamperometry measurements were conducted. As illustrated in Fig. 4f, the overpotential of Fe-MoS_2/CC has negligible increase after 1000 CV cycles. Chronoamperometry exhibits an extremely stale current density at a fixed potential. The XRD, SEM, TEM, and XPS results show that the composition and phase structure have not changed after stability tests (Figs. S21 and S22 in Supporting information). In general, above results prove the excellent long-term stability of Fe-MoS_2/CC electrode.

The above-mentioned electrochemical measurements for M-MoS_2/CC and MoS_2/CC have gained similar results under alkaline media. Fe-MoS_2/CC delivers lower overpotential (194 and 394 mV at the current density of 10 and 50 mA/cm^2, respectively),

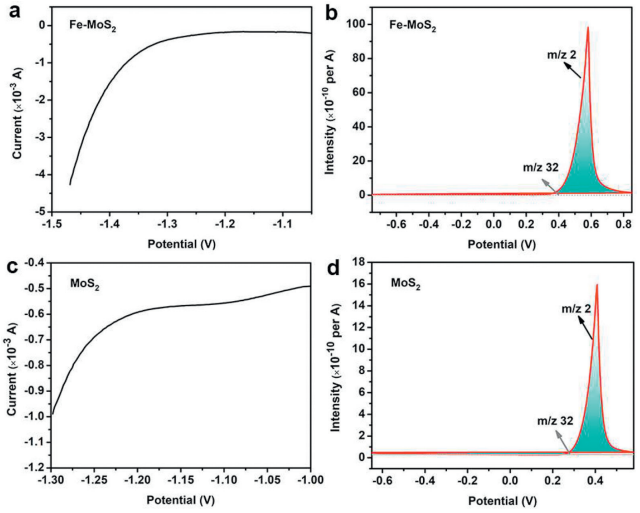

Fig. 5. High pure H_2 generation proved by the *in situ* DEMS analysis. The corresponding *in situ* LSV curves of (a) Fe-MoS_2 and (c) MoS_2. The corresponding faradaic ion current of H_2 for (b) Fe-MoS_2 and (d) MoS_2.

lower Tafel slope (90 mV/dec), smaller R_{ct} value and larger C_{dl} (4.3 mF/cm^2) compared to other M-MoS_2/CC catalysts in 1.0 mol/L KOH, as shown in Figs. S23–S25 (Supporting information). Also the catalytic performance of as-obtained Fe-MoS_2/CC is comparable and even superior to the reported Mo-, Ni- or Co-based HER electrocatalytic materials (Table S4 in Supporting information). The polarization curves and *i-t* curves demonstrate that there is no deactivation for HER. The XRD, SEM, TEM, and XPS measurements (Figs. S26 and S27 in Supporting information) prove that the composition and morphology remain stable after long-term operation. These results verify that the prepared Fe-MoS_2/CC also has superior electrocatalytic durability in 1.0 mol/L KOH aqueous solution and may be a potential highly-active and stable noble metal-based electrocatalyst candidate for HER. The in situ differential electrochemical mass spectrometry (DEMS) measurements were further performed to analyze the gas produced by decoupled alkaline water electrolysis at a sweep rate of 5 mV/s. As shown in Fig. 5, the H_2 evolution for Fe-MoS_2 and MoS_2 catalysts is detected via the online analysis record in parallel with the current in the LSV curves. As shown in Figs. 5b and d, in parallel with the entire electrolysis process, the H_2 was detected, whereas the O_2 remained at the background

level, suggesting no O_2 generation and better selectivity of hydrogen evolution for prepared catalysts. Meanwhile, it is found that the prepared Fe-MoS_2 product shows higher current value than MoS_2 sample in both LSV and DEMS curves, confirming more excellent electrocatalytic H_2 production performance. Furthermore, Fig. S28 (Supporting information) exhibits that the moles of released hydrogen bubbles for Fe-MoS_2 and MoS_2 catalysts were plotted with the coincidence of theoretically calculated value. Correspondingly, both of the catalysts present Faradaic efficiency close to 100% for HER, demonstrating the electrolysis has almost no side effects. Overall, the as-designed M-MoS_2/CC catalysts synthesized from Keplerate polyoxomolybdate as precursors exhibit remarkable electrocatalytic property for HER in both acidic and alkaline media, which is rarely reported on POMs mediated preparation of MoS_2-based catalysts. The main reasons are the integration of homogeneous metal doping modification and highly conductive carbon cloth substrate: (1) Transition metal doping could enlarge the interlayer spacing of MoS_2 and expose more accessible catalytic active sites during the HER process; (2) The introduction of foreign transition metals could tune the surrounding electronic properties of MoS_2, create abundant active sites and efficiently balance of the adsorption and desorption of H; (3) The M-MoS_2 catalysts firmly grown on the highly conductive carbon cloth substrate could accelerate the transmission of electrons and prevent the catalyst from peeling off during the process of catalytic process, thus showing the high electrochemical stability.

In summary, based on the idea of fully exploiting the advantages of POMs to rationally design the highly efficient HER electrocatalysts wide range pH activity, the Keplerate poly-oxomolybdate nanoball were selected as precursors to fabricate the transition metal doped MoS_2 materials (M-MoS_2/CC, M = Fe, Cr and V) by a simple hydrothermal-vulcanization strategy. The highly hydrophilic, solubility and gated pores for these porous spherical molybdenum oxide-based clusters can allow sufficient permeation and transportation of sulfur source in aqueous solution, thus realizing the uniform vulcanization instead of forming separate phases. The homogeneous transition metal doping enlarges the interlayer spacing and effectively tunes the surrounding electronic structure of MoS_2, which could provide more reactive active sites and optimize the adsorption/desorption of active hydrogen species. In addition, the M-MoS_2 catalysts *in situ* growth on CC substrate could enhance the electrons transmission in the whole electrode and prevent the catalyst from peeling off during the process of catalytic process. All these properties guarantee the prepared M-MoS_2/CC to exhibit prominent HER electrocatalytic activity and long-term stability in both acidic and alkaline media, outperforming most of reported typical transition metal sulfide-based catalysts. All things considered, this work may provide a new perspective for rational design and preparation of specific POMs-mediated nanomaterials-modified conductive substrates for energy conversion and storage applications.

Declaration of competing interest

The authors declare that they have no known competing financial interests or personal relationships that could have appeared to influence the work reported in this paper.

Acknowledgments

This work is financially supported by the National Natural Science Foundation of China (Nos. 52171210, 21978110 and 22201097), and the Program for the Development of Science and Technology of Jilin Province (Nos. 20220201130GX and YDZJ202201ZYTS313).

Supplementary materials

Supplementary material associated with this article can be found, in the online version, at doi:10.1016/j.cclet.2023.108930.

References

[1] Z. Zeb, Y.C. Huang, L.L. Chen, et al., Coord. Chem. Rev. 482 (2023) 215058.
[2] T. Wang, M. Xu, F.R. Li, et al., Appl. Catal. B 280 (2021) 119421.
[3] D.V. Jawale, F. Fossard, F. Miserque, et al., Carbon 188 (2022) 523–532.
[4] Z.J. Chen, S.N. Yun, L. Wu, et al., Nano-Micro Lett. 15 (2023) 4.
[5] L. Wang, A.N. Wang, Z.Z. Xue, et al., Chin. Chem. Lett. 34 (2023) 107414.
[6] J. Gautam, Y. Liu, J. Gu, et al., Adv. Funct. Mater. 31 (2021) 2106147.
[7] Q.X. Zhou, C.X. Xu, J.G. Hou, et al., Nano-Micro Lett. 15 (2023) 95.
[8] X.Y. Jia, C. Streb, Y.F. Song, Chem. Eur. J. 25 (2019) 15548–15554.
[9] Z.Y. Tian, X.Q. Han, J. Du, et al., ACS Appl. Mater. Interfaces 15 (2023) 11853–11865.
[10] T. Wang, M. Xu, C.H. Ma, et al., ACS Appl. Mater. Interfaces 13 (2021) 25010–25023.
[11] J.S. Li, Y. Wang, C.H. Liu, et al., Nat. Commun. 7 (2016) 11204.
[12] H.B. Wu, B.Y. Xia, L. Yu, et al., Nat. Commun. 6 (2015) 6512.
[13] M. Shalom, D. Ressnig, X.F. Yang, et al., J. Mater. Chem. A 3 (2015) 8171.
[14] D. Yin, Y.D. Cao, D.F. Chai, et al., Chem. Eng. J. 431 (2022) 133287.
[15] D. Gao, R. Liu, J. Biskupek, et al., Angew. Chem. Int. Ed. 58 (2019) 4644–4648.
[16] Y. Liu, C.L. Yue, F.Y. Sun, et al., Chem. Eng. J. 454 (2023) 140105.
[17] S. Anantharaj, S. Kundu, S. Noda, J. Mater. Chem. A 8 (2020) 4174–4192.
[18] L. Ye, Y. Du, Y. Zhao, et al., ACS Appl. Nano Mater. 3 (2020) 8372–8381.
[19] B. Hinnemann, P.G. Moses, J. Bonde, et al., J. Am. Chem. Soc. 127 (2005) 5308–5309.
[20] J.T. Zhang, L.M. Dai, Nitrogen, et al., Angew. Chem. Int. Ed. 55 (2016) 13296.
[21] Y. Hou, H.J. Pang, J.J. Xin, et al., Adv. Mater. Interfaces 7 (2020) 2000780.
[22] B. Chen, P. Hu, F. Yang, et al., Small 19 (2023) 2207177.
[23] W.D. Zhou, M.Y. Chen, M.M. Guo, et al., Nano Lett. 20 (2020) 2923–2930.
[24] D.J. Zang, H.Q. Wang, Polyoxometalates 1 (2022) 9140006.
[25] Y.K. Lua, X.X. Guo, L.Y. Yang, et al., Chem. Eng. J. 394 (2020) 124849.
[26] Y.C. Huang, Y.H. Sun, X.L. Zheng, et al., Nat. Commun. 10 (2019) 982.
[27] Y.J. Tang, Y. Wang, X.L. Wang, et al., Adv. Energy Mater. 6 (2016) 1600116.
[28] C. Schäffer, A. Merca, H. Bögge, et al., Angew. Chem. Int. Ed. 121 (2008) 155–159.
[29] H. Taghiyar, B. Yadollahi, Sci. Total Environ. 708 (2020) 134860.
[30] T. Wang, T. Ji, W.L. Chen, et al., Nano Energy 68 (2020) 104349.
[31] Y.H. Feng, Z. Zhao, T. Wang, et al., Ceram. Int. 48 (2022) 20062–20069.
[32] T. Wang, M. Xu, X.H. Li, et al., Inorg. Chem. Front. 7 (2020) 1676.
[33] H.Q. Yin, L.L. Yang, H. Sun, et al., Chin. Chem. Lett. 34 (2023) 107337.
[34] Y.L. Zhang, C.W. Jia, R.N. Tian, et al., Rare Met. 40 (2021) 1578–1587.
[35] J.Y. Zhang, Z.K. Zhao, Q. Li, et al., Adv. Powder Mater. 2 (2023) 100113.
[36] F.R. Li, H.R. Liu, W.C. Chen, et al., Inorg. Chem. Front. 9 (2022) 3828.
[37] Y.M. Zhao, X.X. Wang, Z. Li, et al., Chin. Chem. Lett. 33 (2022) 1065–1069.
[38] M. Zhang, B.L. Yang, T. Yang, et al., Chin. Chem. Lett. 33 (2022) 362–367.
[39] Y.Q. Shao, K.K. Feng, J. Guo, et al., J. Adv. Ceram. 10 (2021) 1025–1041.
[40] Q. Liu, M.Y. Li, Y.M. Shi, et al., Rare Met. 41 (2022) 836–843.
[41] X.X. Li, X.C. Liu, C. Liu, et al., Tungsten 5 (2023) 100–108.
[42] J. Liu, S.L. Wang, J.L. Xuan, et al., Tungsten 4 (2022) 38–51.
[43] C.Y. Yin, Q. Li, J. Zheng, et al., Adv. Powder Mater. 1 (2022) 100055.
[44] L. Zhang, Z.H. Hu, J.T. Huang, et al., J. Adv. Ceram. 11 (2022) 1294–1306.